Characteristics of Wall Pressure in Axisymmetric Swirling Pipe Flow and Non-Axisymmetric Swirling Pipe Flow with Initial Segmental Wake Component: In A Straight Pipe

Kiattisak Kobkanjanakorn and Asi Bunyajitradulya
Fluid Mechanics Research Laboratory, Department of Mechanical Engineering
Faculty of Engineering, Chulalongkorn University
Bangkok 10330, Thailand
Tel. 02-218-6645; Fax. 02-252-2889
Email: basi@chula.ac.th
URL: http://www.eng.chula.ac.th/~fmeabj

Abstract

Axisymmetric swirling pipe flow and non-axisymmetric swirling pipe flow with initial segmental wake component in a straight pipe are studied. The swirling flows are generated by a rotating pipe, and the initial segmental wake component by a segmental annular tab. Focus is placed on the characteristics of wall pressure distribution. The investigated flows have a pipe Reynolds number of 3.7×10^4 and swirl ratios ranging from 0 (no swirl) to 1.8. The results for axisymmetric cases show that, unlike a non-swirling flow, a swirling flow exhibits a non-linear pressure drop in the initial region, with initially fast rate of drop gradually decreasing and approaching linear drop. The minor loss coefficient associated with swirl is found to be proportional to the square of swirl ratio. On the other hand, for non-axisymmetric cases, the results show that the degree of non-uniformity in wall pressure generated by the tab varies with swirl ratio: higher swirl generates higher strength of non-uniformity, the result which can be attributed to an increase in effective velocity approaching the tab. This non-uniformity in wall pressure, traced by the minimum in wall pressure, travels downstream in a swirling motion in the same direction as the swirl. The results also show that, the recovery length to uniformity varies with the square of swirl ratio; the decay of the maximum difference in wall pressure can be approximated by a power law of downstream distance, with the decay rate being an exponential function of swirl ratio; and in case of maximum swirl (swirl ratio of 1.8) the decay of swirl ratio for wall pressure (Sr_p) can be approximated by an inverse function of downstream distance.

1. Introduction

Internal swirling flow can be found in many engineering applications. Some are intentional such as swirling flows in combustors and heat exchangers. In these cases, swirl is introduced intentionally in order to achieve certain desired effects such as mixing enhancement and heat transfer augmentation. On the other hand, some occur as a side effect of main flow configuration; in other words, they are secondary flows. Examples in this category are swirling flows in a pipe downstream of turbomachines and pipe bends. These flows can often cause noise and vibration (Murakami, 1961).

Two configurations of internal swirling flow were the main focus in the past: swirling flows through pipe and annular swirling flows. This study focuses on the former. Past studies have made some considerable progress towards the understanding of the characteristics of *axisymmetric* turbulent swirling flow through a straight pipe. Of particular interest and relevant to this study and many applications are the relaxation and decay characteristics of various flow properties. Kreith and Sonju (1965) studied swirl by using twisted tape as swirl generator and measuring average swirl with a swirl vortex meter. It was found that swirl decayed to approximately 10-20 % of its initial

RECEIVED 9 AUGUST, 2001
ACCEPTED 14 NOVEMBER, 2001

value in a distance of approximately 50 diameters downstream of the introduction of swirl and that the decay was more rapid for smaller Reynolds number. Kitoh (1991) studied swirl by using guide vanes as swirl generator and determining swirl from velocity data obtained by a three-hole pitot tube. It was found that, swirl intensity (defined as a non-dimensional angular-momentum flux along the pipe axis) decayed downstream as a result of wall friction, and the decay rate was found to be exponential with coefficient depending on swirl intensity along the pipe axis. Parchen and Steenbergen (1998) studied swirl by using guide vanes as swirl generator and determining swirl from velocity data obtained by a laser-doppler velocimeter (LDV). The effect of initial velocity distribution on the decay rate of swirl was investigated. Two initial distributions, referred to as 'concentrated vortex' and 'distributed vortex' profiles and differed in both axial and azimuthal velocity components, were generated using a streamlined, axisymmetric centerbody. It was found that the decay rate was exponential and depended on the initial distribution even far downstream from the swirl generator. In comparison, swirling flow with distributed vortex profile decayed by approximately 20% faster than that with the concentrated vortex profile. Weske and Sturov (1974) studied swirl by using a rotating pipe with honeycomb as swirl generator and measuring mean and turbulence velocities with hot-wire anemometer. It was found that longer recovery length was required for turbulence quantities to attain fully-developed condition in comparison to that of mean quantities. Specifically, their results showed that the recovery length for the turbulence field in excess of 100 diameters was required for the flow with swirl number of one. Yajnik and Subbaiah (1973) studied swirl by using guide vanes as swirl generator and measuring mean quantities with pressure probes. The effect of swirl on flow development and the similarity laws were investigated. It was found that the mean velocity profiles admitted similarity laws at sufficiently high Reynolds number; the wall law was not sensibly dependent on swirl, while the velocity defect law was sensitive to swirl. In addition, the logarithmic skin-friction law was admitted with the additive coefficient depending linearly on swirl.

Other related aspects of swirling flow through a straight pipe were studied, for example, by Anwer and So (1989) who studied stabilizing and destabilizing effects of swirl; Miau et al. (1996), effect of swirl in circular-to-rectangular transition ducts; Wang and Rusak (1996, 1997a, 1997b), Rusak et al. (1997), and Rusak (1998), stability analysis and vortex breakdown; Murakami and Kikuyama (1980), Kikuyama et al. (1983), Orlandi and Fatica (1997), axially rotating pipe; and many others (e.g., Rochino and Lavan, 1969; Kobayashi and Yoda, 1987; Holzäpfel et al., 1999; Wu et al., 2000).

On the other hand, internal flows, swirling or not, may be obstructed by a segmental blockage such as pipe fittings and valves. As a result, the flow characteristics are modified and an obvious casualty is the loss of axisymmetry. This non-axisymmetry most certainly will be more 'amplified' in a swirling flow than in a non-swirling one in the sense that it will sustain farther downstream owing to the centrifugal stability of the former, resulting in a *non-axisymmetric* swirling flow. Non-axisymmetric swirling flows can also be generated naturally from non-swirling flows; in such case, examples are flows through pipe bends and valves. In terms of engineering applications, the non-axisymmetry can result in uneven loading on piping structure, vibration and noise, and error in measurements of flow properties such as flowrate and static pressure. The latter has direct impact on correct use of flow measurement devices such as the installation and use of pressure gauge, orifice meter, venturi meter, etc.

Even though non-axisymmetric internal flows are commonly found in engineering applications, surprisingly few studies have addressed the issue and even fewer for non-axisymmetric swirling flows. In this respect, Sparrow et al. (1979) studied the effect of a

segmental blockage in a fully-developed turbulent pipe flow. It was found that the minor loss coefficient depended strongly on the blockage ratio and was insensitive to Reynolds number. Relatively large circumferential pressure variation was found near the blockage but died away with increasing downstream distance; circumferential uniformity was attained within the downstream distance of 6-8 diameters for the blockage ratio of ¼ and 8-12 for ½. The highest pressure was found on the opposite-blockage wall near the blockage and moved opposite to the blockage wall farther downstream. This change in position of the highest pressure was attributed to the corresponding change in streamline curvature as the flow contracted to circumvent the blockage and subsequently expanded to fill the cross section farther downstream. In addition, the axial pressure distribution was found to display a drop and a subsequent recovery due to the acceleration-deceleration sequence experienced by the deflected flow. In the spirit of improving the performance of an orifice meter, Ouazzane and Barigou (1999) studied the use of vanes and a porous plate for removing non-axisymmetric swirl generated by a ball valve.

Owing to its importance both in terms of academic and application, this study aims at the investigation of the characteristics of *non-axisymmetric* swirling pipe flows. The non-axisymmetry in the form of segmental wake component is generated in the initial profile with a segmental annular tab, resulting in non-uniformity in wall pressure distribution along the circumference. The decay characteristics of this non-uniformity is then investigated at various swirl ratios. For comparison, the corresponding axisymmetric swirling pipe flows, i.e., without blockage, are also investigated. This study is the continuation of our previous work, Kobkanjanakorn and Bunyajitradulya (1998).

2. Experimental Setup

The experiments are conducted in the Fluid Mechanics Research Laboratory, Department of Mechanical Engineering, Faculty of Engineering, Chulalongkorn University. The experimental setup is shown schematically in Fig. (1).

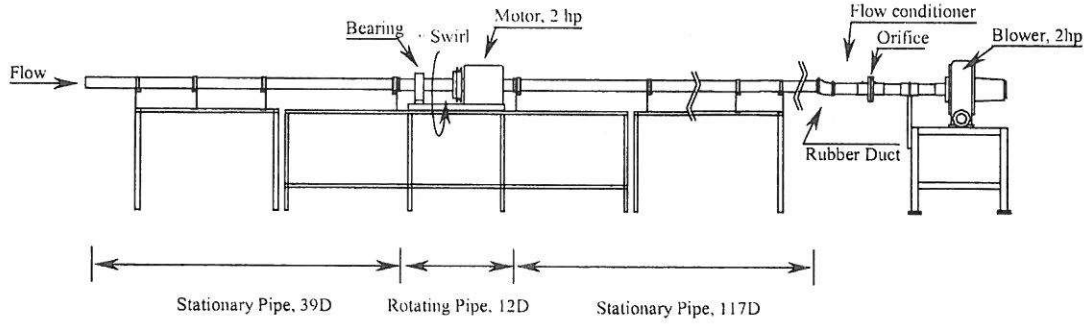

Fig. 1. Experimental setup.

The setup is basically a pipe flow setup with four sections: upstream stationary pipe, rotating pipe, downstream stationary pipe, and flow monitoring and blower sections. The upstream and downstream stationary pipe sections are made from acrylic pipe sections; each with inner diameter (D, radius R) of 74 mm and outer diameter of 80 mm, and length of 962 mm. The upstream section has a total pipe length of $39D$ (3 acrylic pipe sections);

the downstream section, 117*D* (9 acrylic pipe sections). Pipe sections are connected together via couplings made from acrylic pipe with inner diameter of 80 mm, equal the outer diameter of the sections, and outer diameter of 90 mm. This helps minimizing misalignment. Sealing at the couplings is by silicone sealant.

Swirling motion is imparted to air flow inside the pipe via the rotating pipe section which is made from steel pipe with inner diameter of 74 mm and length of 888 mm (12*D*). As shown in Fig. (2), in order to impart swirl effectively, two sets of honeycomb made from plastic drinking straws (inner diameter of 6 mm and length of 148 mm) is placed at the upstream end. The upstream honeycomb is covered with a household screen (mesh 16) at each end; the downstream one, a household screen at the upstream end and a mesh-30 screen at the downstream end. Further flow conditioning is provided by a series of four mesh-30 screens spaced uniformly at 100 mm apart. The last screen is placed at 128 mm from the rotating pipe exit. The rotating pipe section is driven by a belt-pulley and 2hp-motor-inverter system; thus, rotational speed can be adjusted. Sealing between the rotating pipe section and the stationary pipe sections is by V-rings.

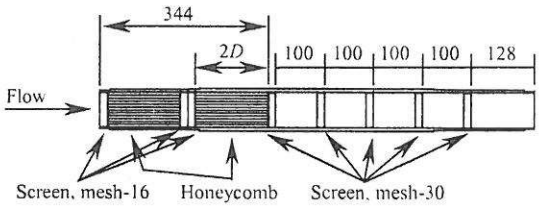

Fig. 2. The rotating pipe section.

Downstream of the downstream stationary pipe section are connected a rubber tube which is used for isolating vibration from the blower; flow conditioner (honeycomb and screens), for conditioning flow before entering an orifice; an orifice, for monitoring flowrate; another flow conditioner (screens), for preventing the upstream effect (induced swirl) of the blower; and a 2-hp centrifugal blower, for driving the setup.

Two sets of flow conditions are investigated: axisymmetric and non-axisymmetric flows. The non-axisymmetry is generated by a *stationary* segmental annular tab, shown in Fig. (3) together with the coordinates system employed. The segmental annular tab is made from aluminum plate with height of *R*/2, base of 90°, and thickness of 0.4 mm. This corresponds to a blockage ratio, *B*, of 3/16 or 0.19. The tab is glued to a stationary acrylic ring, 3 mm in width and equal diameters to those of the stationary pipes, and placed at an angular position $\theta = 180^\circ$ between the rotating pipe exit and the stationary pipe inlet. The streamwise position of the tap is designated to be the origin of the coordinates system, i.e., $x = 0$.

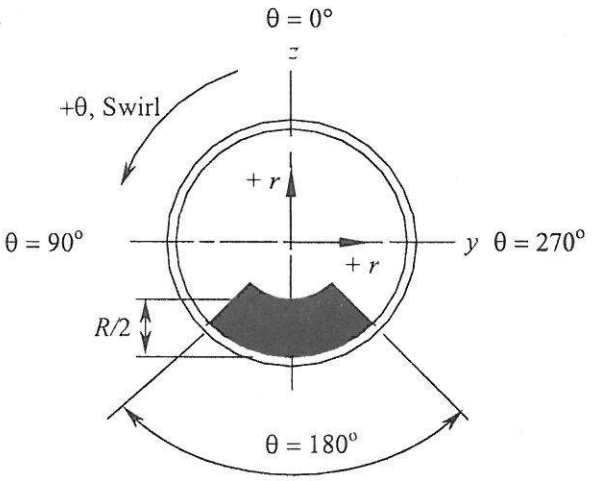

Fig. 3. The tab and the coordinates system as viewed towards upstream.

For each set of experiments, a total of 6 *swirl ratios* (*Sr*), defined as the ratio of the peripheral velocity of the pipe (ΩR) to the bulk mean axial velocity of the flow ($\bar{u}$), are investigated: $Sr = 0$ (no swirl), 0.3, 0.6, 0.9, 1.2, and 1.8. Note that swirl can also be defined more rigorously in terms of the *swirl*

number (*Sn*), defined as the ratio of the axial flux of angular momentum to the axial flux of axial momentum divided by the pipe radius:

$$Sn = \frac{\int_0^R u_\theta u_x r^2 dr}{R\int_0^R u_x^2 r dr}, \qquad (1)$$

where u_x (or u) and u_θ (or w) are the streamwise and tangential velocity components, respectively. However, in this study, for simplicity and for the fact that the rotating pipe - to which no-slip condition is naturally applied at the periphery - is employed as a swirl generator, we shall adopt the swirl ratio as the measure of swirl. The experiments are conducted at the bulk mean velocity measured at the rotating pipe exit of 7.8 m/s, corresponding to a Reynolds number (Re) based on the pipe diameter of 3.7×10^4. For convenience, these experimental cases shall be designated as Srxx(T), where xx denotes the decimal of the swirl ratio and the suffix "T" denotes the non-axisymmetric case, i.e., the case with tab. For example, Sr18 and Sr18T denote the cases with swirl ratio of 1.8, and without and with tab, respectively.

In order to establish experimental conditions, a set of velocity and pitot-pressure measurements is made and summarized in Table (1). In these measurements, the pitot and cobra probes, which are built and calibrated in-house, are used. Both are made from hypodermic needles of inner and outer diameters of 0.8 and 1.25 mm, respectively. The cobra probe has an apex angle of 37°. For further details regarding the design, calibration, and use of a cobra probe; see Chue (1975).

Static pressure distribution is measured with wall static pressure taps. The locations of the tap and the corresponding spatial resolutions are as follows: $0.5 \le x/D \le 6.0$, every $0.5D$ and 15°; $7 \le x/D \le 38$, $1D$ and 30°; $41 \le x/D \le 76$, $2D$ and 45°. All the pressure-difference readings, including those of the probes measurement, are provided by an inclined manometer with 0.2 mm WG resolution.

x/D	Quantity	Probe	Remark
-31	velocity (x)	pitot	all cases, along y-axis
0.5	velocity (x)	pitot	Sr00 (w/o swirl), along y- and z- axes
	velocity (x,θ)	cobra	Srxx (w/ swirl), along y- and z- axes
	pitot p.	pitot	all cases, along y- and z- axes
Orifice	velocity (x)	pitot	all cases, 2D upstream of the orifice inlet, along y- and z- axes

Table 1. Measurements of experimental condition.

Finally, to give some indication of the uncertainty in measurements, we give an overall estimate of uncertainty (Kline, 1985) in measurements of axial velocity using the pitot probe, and axial and tangential velocities using the cobra probe to be well within $\pm$ 0.3 m/s.

3. Results and Discussion

Results are divided into three sections: the results for initial conditions, axisymmetric swirling flows, and non-axisymmetric swirling flows. The details are as follows.

3.1. Initial conditions

Measurements of the velocity profile along the y-axis upstream of the rotating pipe inlet (x/D = -31) indicate that the flows are fairly symmetric with respect to the center and approaching fully-developed for all cases. Besides the knowledge of the initial state of the flow before it enters the rotating pipe, the measurements at this location are conducted in order to estimate leakage at various sections of the setup. Except for case Sr18, the bulk mean velocities determined from integration of the profiles at this location are found to be within the range of 7.9-8.0 m/s for all cases. For case

Sr18, the bulk mean velocity at this location is measured to be 7.3 m/s for the same flowrate monitored at the rotating pipe exit and at the orifice. This indicates some leakage into the setup, the issue we shall further discuss below. Note that case Sr18 has the highest rotational speed.

Figure (4) shows the initial velocity profiles (at the rotating pipe exit, $x/D = 0.5$) traversed along the y- and z-axes for cases without tab. The axial velocities shown in Fig. (4a) are normalized by the bulk mean velocity at this location, which ranges within 7.7-7.8 m/s for all cases. All the initial profiles are fairly top-hat with boundary layer thickness of approximately $0.3R$. Except for cases Sr12 and Sr18, the profiles are fairly uniform outside the boundary layer, with variations along the radial direction within any one case and from case to case less than $\pm$ 0.05. However, cases Sr12 and Sr18, in which the rotational speeds are higher, slightly deviate from others but still lie within $\pm$ 0.1. The tangential velocities outside the boundary layer shown in Fig. (4b) have the characteristics of a rigid-body rotation, with the boundary layer thickness varying from case to case but all of less than $0.3R$. The speed of rigid-body rotation in the core is closed to the corresponding rotating-pipe speed distribution, shown as solid line in the figure. Except for case Sr03, in which the value of 8% is found, the angular velocities in the core for all cases are found to deviate by less than 2% from the corresponding angular velocities of the pipe. Thus, a forced-vortex type velocity distribution is achieved in the central 70% region of the pipe in this experiment.

Owing to the presence of the tab, the initial velocity profiles approaching the tab for cases with tab cannot be measured, and they are presumed to be the same as the corresponding profiles of cases without tab under the same flowrate monitored at the orifice and the same rotational speed of the rotating pipe.

The measurements of the velocity profiles upstream of the orifice show the bulk mean velocities of 7.8-8.1 m/s for all cases. From the data of the bulk mean velocities at the three locations, i.e., upstream and downstream of the rotating pipe, and upstream of the orifice, it can be determined that leakage for all cases, except case Sr18, is well within 3%. For case Sr18, in which the rotational speed of the pipe is highest, the result indicates leakage of 6% between the upstream and downstream ends of the rotating pipe. Most likely, the leakage occurs at the V-rings.

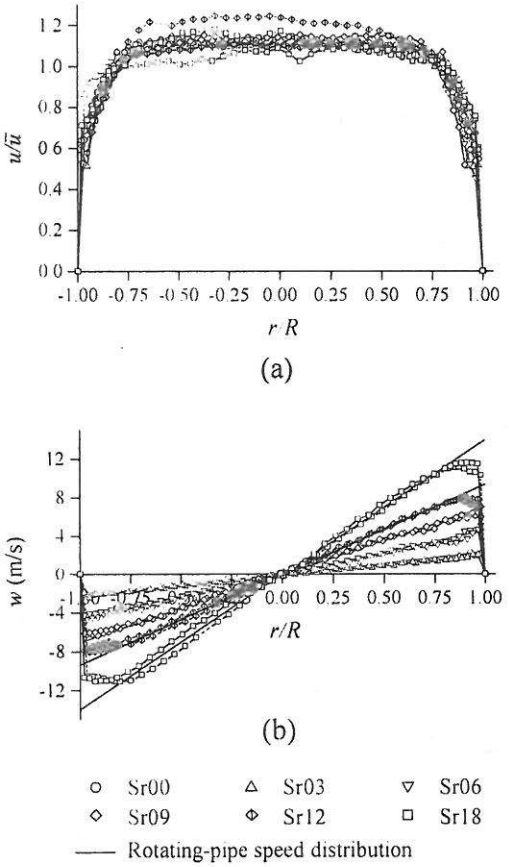

Fig. 4. Initial velocity profiles (at $x/D = 0.5$) along y- and z-axes for cases without tab: (a) axial components, (b) tangential components. Markers with dashed lines indicate those along the y-axis; with solid lines, along the z-axis.

In order to establish the initial conditions, the distributions of pitot pressure along the y- and z-axes at the rotating pipe exit ($x/D = 0.5$)

are surveyed in all cases and the results are plotted in Figs. (5) and (6) as the coefficient of pitot pressure, C_{PT}, defined as

$$C_{PT} = \frac{P_T - P_{ref}}{\frac{1}{2}\rho\bar{u}^2}, \qquad (2)$$

where ρ is density, P_T is pitot pressure, and P_{ref} is reference pressure, which is taken to be the wall pressure at $x/D = 0.5$ and $\theta = 0^o$. Note that P_{ref} is not constant but varies from case to case. Figure 5 shows the distributions of C_{PT} along the y- and z-axes for cases without tab. The results show fairly symmetric distributions of pitot pressure, further indicate that the flows are axisymmetric. For cases with swirl, a local minimum value of C_{PT} is found at the center, and for all cases the boundary layer is observed along the pipe wall. The maximum difference in C_{PT} along the axes and outside the boundary layer is found to increase with swirl ratio, from virtually 0 in case Sr00 to the maximum value of approximately 1.6 in case Sr18. Also in the figure, the readings of a pitot probe, if it is assumed to response only to an axial velocity component, in a forced-vortex flow with uniform axial-velocity distribution are shown as dashed lines for comparison. The equation for these lines are $C_{PT'}(r) = C_{PTC} + (\Omega r/\bar{u})^2$, where $C_{PT'}$ is the forementioned pitot-pressure coefficient and C_{PTC} is the corresponding value at the center. The experimental data at the center of the pipe were used as reference values in the equation.

Figure (6a) shows the distributions of C_{PT} along the z-axis for cases with tab. Naturally, the results show wake behind the tab for all cases, the pitot pressure on the negative-z side is lower than that on the positive-z side. Thus, unlike the cases without tab in Fig. (5), the flows in these cases are non-axisymmetric. At this point, it is appropriate to mention that, for cases with swirl, it is expected that the wake generated by the tab will be convected in the direction of local velocity ($\bar{u} + \bar{w}$), i.e., more or less along local swirl helix.

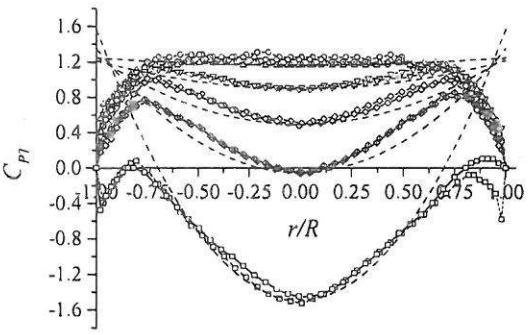

Fig. 5. Coefficient of pitot pressure at x/D = 0.5 for cases without tab. For legends, see Fig. 4; for dashed lines, see text

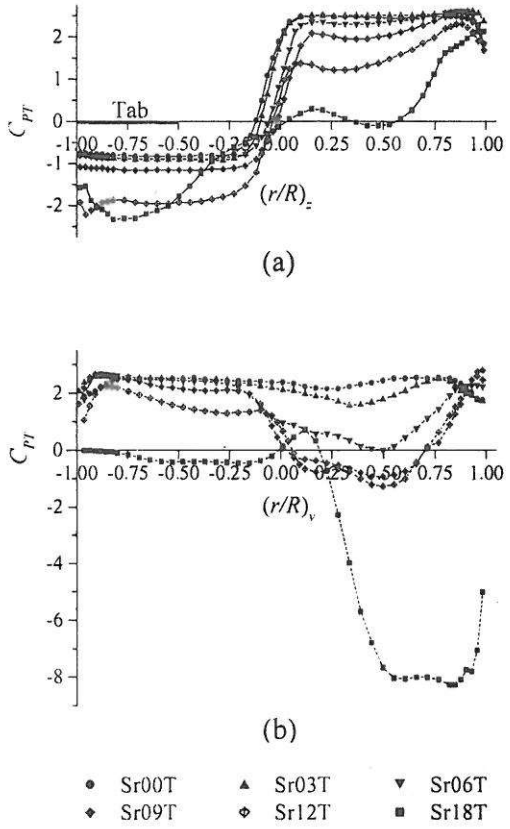

Fig. 6. Coefficient of pitot pressure for cases with tab: (a) along z-axis, (b) along y-axis.

Furthermore, from the figure, some interesting points can be observed. The

maximum difference in C_{PT} between the two sides along the axis depends on swirl ratio and it varies approximately from 3 at low swirl to 5 at high swirl, significantly larger than the corresponding values found in cases without tab in Fig. (5). This is a rough indication of the strength of the wake generated and of the variation of the strength with swirl ratio and can be explained in terms of the drag of the body. Higher swirl causes increase in effective impinging velocity ($\vec{u} + \vec{w}$) on the tab on the one hand but decrease in apparent area of the tab on the other. Simple and approximate analysis of a drag on a flat plate shows that the effect of an increase in effective velocity overtakes that of a reduction in apparent area in the range of parameters in this experiment. However, the variation of the drag coefficient with angle of attack and, equally important, the response of the pitot probe to yaw angle need to be taken into account, the issue that does not concern us in this experiment and we shall leave it at this. Additionally, at low swirl an abrupt change in pitot pressure near $r/R = 0$ is observed while at high swirl a more gradual change is observed. At low swirl, the region of abrupt change corresponds to the edge of the wake. Thus, it is seen that the transverse extent of the wake is thicker than the height of the tab. This can be attributed to edge separation over the top edge of the tab. The reason for the more gradual change in C_{PT} at high swirl will become clearer in Fig. (6b).

Continuing from Fig. (6a), Fig. (6b) shows the distributions of C_{PT} along the y-axis for cases with tab. In case Sr00T, in which there is no swirl, the pitot pressure is, as expected, fairly constant throughout the central region of the pipe. As swirl increases, however, the pitot pressure on the positive-y side is progressively lower than that on the negative-y side. The maximum difference in C_{PT} between the two sides along the axis is observed in case Sr18T at the value of approximately 9, higher than the corresponding value found along the z-axis and than that found in the case without tab in Fig. (5). This is a result of the convection of the wake along helical path due to swirling motion and it is illustrated in Fig. (7). Also shown in this figure are the presumed angular positions of the wake at $x/D = 0.5$ for all cases with swirl, if it is assumed that swirl does not decay. In such case, the center of the tab wake for case Sr18T lies approximately along the positive-y axis, in accordance with the relatively lower pitot pressure observed along the positive-y axis in Fig. (6b) in comparison to the relatively higher pitot pressure observed along the negative-z axis in Fig. (6a). In addition, as a result of this convection, the more gradual change in pitot pressure along the z-axis is observed in Fig. (6a) and transforms into the more abrupt change along the y-axis in Fig. (6b). In this regard, these trends in the distribution of pitot pressure for other swirling cases may be less obvious, which are due to many factors such as the strength of the wake generated, the presumed angular position of the wake at current position, the initially fast decays of the wake and of the swirl, and the growth of the wake.

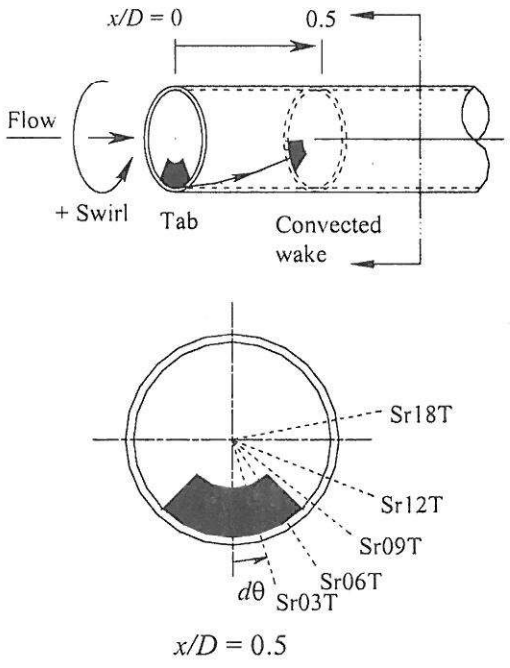

Fig. 7. Illustration of convection of the tab wake due to swirling motion and the angular position of the tab at $x/D = 0.5$.

3.2. Wall pressure distribution: Axisymmetric flows

Figure (8), see back, shows initial sequence, $0.5 \le x/D \le 3.0$, of polar plots of wall pressure distribution for cases without tab. The plots are given in terms of the *local coefficient of wall pressure* (C_{Pref}), defined as

$$C_{Pref} = \frac{P - P_{ref}}{\frac{1}{2}\rho\bar{u}^2}, \qquad (3)$$

where P is local wall pressure and P_{ref} is local reference pressure which is taken as the local wall pressure at $\theta = 0^o$. The uncertainty in C_{Pref} is estimated to be within $\pm$ 0.05. Therefore, in this experiment the wall pressure is deemed to be uniform at a cross section when C_{Pref} at that cross section has values at all angular positions within the interval (-0.05, 0.05).

From Fig. (8), it can be seen that, within the experimental uncertainty, the wall pressure for all cases is fairly uniform right at the rotating pipe exit, except for case Sr09. In case Sr09, slight non-uniformity of magnitude of 0.3 is observed but soon dies down at x/D = 2.5. This non-uniformity was found to be caused by slight bump at the coupling at the rotating pipe exit, we leave it here to give some rough indication of the effect of the bump. Note that, in conducting the experiment, when the pressure is found to be uniform at a cross section, detailed measurements along the circumference are made further downstream by at least 5 diameters in order to ensure that the pressure distribution has reached uniformity. After that, only the pressure at $\theta = 0^o$ is measured.

In order to evaluate the effect of swirl on average pressure drop, the *global coefficient of wall pressure* ($C_{Pref'}$) is defined,

$$C_{Pref'} = \frac{P - P_{ref'}}{\frac{1}{2}\rho\bar{u}^2}, \qquad (4)$$

where P is local pressure and $P_{ref'}$ is reference pressure which is taken to be at x/D = 0.5 and $\theta = 0^o$. Then the values of $C_{Pref'}$ are averaged over the circumference, $\overline{C_{Pref'}}$. Figure 9 shows the distributions of $\overline{C_{Pref'}}$ along the pipe axis for all cases without tab. Note that $P_{ref'}$ is not constant but varies from case to case; therefore, Fig. (9) should be viewed only in a differential sense.

The distribution of $\overline{C_{Pref'}}$ in case Sr00 (no swirl) shows characteristics of a linear drop. As swirl is imparted, however, $\overline{C_{Pref'}}$ shows fast decay rate initially, then the decay rate gradually becomes slower and approaches a linear drop; the higher the swirl, the faster the initial drop. This effect is most amplified and easily seen in this figure in case of the highest swirl, Sr18. This characteristics of pressure drop can be attributed to the decaying of swirl, or tangential velocity, and suggests that the decay rate of swirl is not a constant but a function of swirl number as previously found by former workers (see, e.g., Kitoh, 1991).

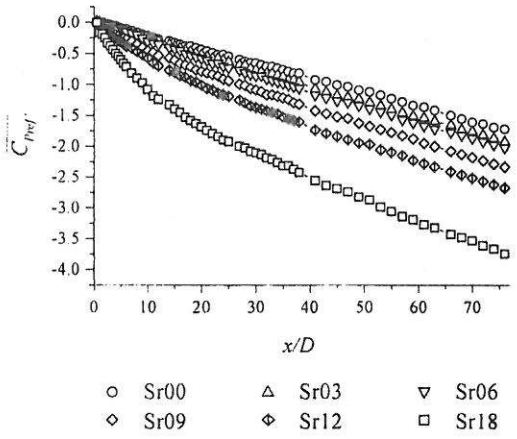

Fig. 9. Distribution of $\overline{C_{Pref'}}$ along pipe axis.

In addition, near the end of the measurement station, all swirling cases, except maybe Sr18, have slope approximately equal to that of Sr00, signifying that the flows are approaching fully-developed, at least as far as

pressure is concerned. For case Sr18, slight deviation in slope can still be observed near the end. Nonetheless, given that the slope for all cases is expected to level up and approach that of Sr00 and all the lines are expected to become parallel, the minor loss coefficient K for cases with swirl can then be approximated by the deviation in $\overline{C_{Pref}}$ from that of case Sr00 at any downstream location. As a result, we take the last station as the point of evaluation and evaluate the minor loss coefficient as a function of Sr as shown in Fig. 10. The fit in this figure can best be described by the polynomial of degree two, $K = 0.63Sr^2 - 0.097Sr + 0.17$. In other words, the minor loss is found to be proportional to the square of swirl ratio, $K \sim Sr^2$. As past results suggest, e.g., Sparrow et al. (1979), the coefficients in the minor loss equation shown above are expected to be weak functions of Reynolds number.

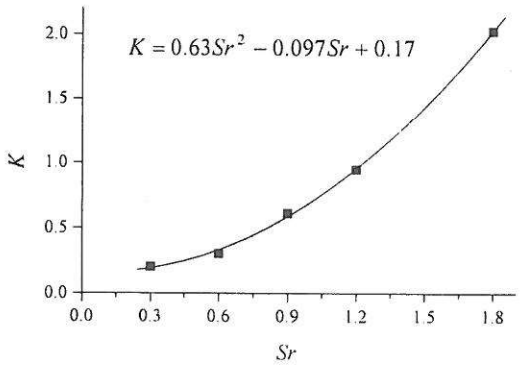

Fig. 10. Minor loss coefficient for cases without tab.

3.3. Wall pressure distribution: Non-axisymmetric flows

Figures 11(a) and (b), see back, show initial sequences of polar plots of wall pressure distribution for cases with tab. Figure (11a) shows those of cases Sr00T, Sr03T, and Sr06T. As a note, in case Sr00T, the change in position of the maximum pressure from opposite-blockage wall to blockage wall as observed by Sparrow et al. (1979) is evident. At x/D = 0.5, the non-axisymmetry in the distribution of wall pressure owing to the wake generated by the tab is pronounced in all cases. The maximum differences in wall pressure along the circumference,

$$\Delta C_{Pref} \max = C_{Pref,max} - C_{Pref,min}, \quad (5)$$

are found to increase with swirl ratio and to be in the order of 0.7 to 0.8 times the bulk dynamic pressure. The fact that ΔC_{Pref} max increases with swirl ratio confirms the result found earlier in pitot pressure, Fig. (6), that higher swirl generates stronger wake. In addition, the angular position of the point of minimum pressure in case Sr00T is found to locate near θ = 180°, the position behind the tab, while those in cases Sr03T and Sr06T are found to move slightly towards θ = 210°, i.e., in the direction of swirl. As flow progresses downstream, the point of minimum pressure is observed to continue to rotate in the direction of swirl. In addition, the maximum difference in wall pressure decays, with the wall pressures reaching uniformity at x/D = 3.0, 5.0, and 5.5 in cases Sr00T, Sr03T, and Sr06T, respectively. In other words, the flow with higher swirl requires longer recovery length for the wall pressure to reach uniformity. These results will become more obvious when we discuss next the results for cases of higher swirl, in which these effects are amplified.

Figure (11b) shows the results for cases of higher swirl: Sr09T, Sr12T, and Sr18T, and Sr00T for comparison. In these cases, because of higher swirl, the wake generated by the tab has higher strength. At x/D = 0.05, for example, the maximum differences in wall pressure along the circumference, ΔC_{Pref} max, are in the orders of 1.0, 1.6, and 3.0 times the bulk dynamic pressure in cases Sr09T, Sr12T, and Sr18T, respectively. In addition, the point of minimum pressure is clearly rotating away from the tab position (θ = 180°) and in the same direction as the swirl. As flow progresses further downstream, however, the rate of rotation is found to decrease significantly and progressively from the initial swirling rate.

This can be seen from the *lagging* of the angular position of the point of minimum pressure behind that following the initial swirl helix, illustrated as radial dashed lines at x/D = 0.5 and 1.0. At this point, it needs to be emphasized that this is the result from the tracing of wall pressure, not of velocity. Hence, even though the trend for velocity is expected to be similar, it is not replaceable. Furthermore, the maximum difference in wall pressure decays, with the wall pressures reaching uniformity at x/D = 14, 25, and 50 in cases Sr09T, Sr12T, and Sr18T, respectively; i.e., the flow with higher swirl requires longer recovery length. The recovery lengths to uniformity, L_u, for all cases are then plotted as a function of swirl ratio in Fig. (12). The best fit is found to be $L_u / D = 15.5Sr^2 - 1.6Sr + 3.0$. That is, the recovery length is proportional to the square of swirl ratio, $L_u \sim Sr^2$. Generally, the coefficients in this equation are expected to be strong functions of blockage ratio B as the result of Sparrow et al. (1979) suggests.

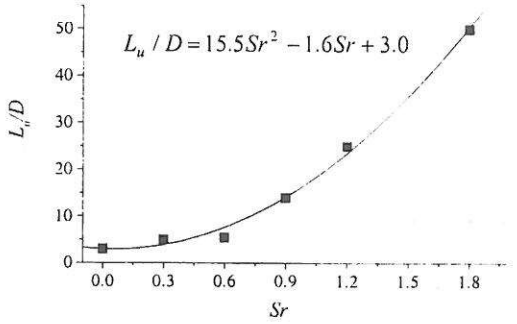

Fig. 12. Recovery length for cases with tab.

In order to gain some insights into the decay of the swirling motion of wall pressure, the period of the angular motion and the decay of the amplitude of wall pressure non-uniformity are investigated. In this regard, the period of the angular motion of wall pressure non-uniformity is investigated by tracing the angular position of the point of minimum pressure (θ_{min}) along downstream distance, and the results for cases Sr09T, Sr12T, and Sr18T are shown in Fig. (13). Owing to small difference and fast decay in wall pressure non-uniformity, the results for cases of low swirl are more difficult to trace and, thus, not shown. Figure (13) also shows the corresponding traces of angular position following the initial swirl helix as dashed lines. It is obvious in all cases shown that the period of the angular motion of the point of minimum pressure gradually stretches along the downstream distance, indicating the decay of swirl. Starting from the tab, the swirling motions of the point of minimum wall pressure last for 2, 4, and 7 periods in cases Sr09T, Sr12T, and Sr18T, respectively.

Furthermore, in order to investigate in detail the gradual decay of swirl, case Sr18T is chosen for its larger number of periods. Then, by evaluating the periods (T) between adjacent angular positions θ_{min} at peaks, and at θ = 120° and 240°, and assigning these periods to the corresponding mid point as illustrated in Fig. (13c), we obtain the relation between the period and streamwise position as shown in Fig. (14). The figure shows an approximate linear relation between the period and the streamwise location, with the linear fit given by $(T / D) = 0.1(x / D) + 5.4$. Hence, if we define the swirl ratio for the swirling motion of wall pressure non-uniformity, Sr_p, as the ratio between the angular velocity and the axial velocity of the point of minimum pressure, i.e., $Sr_p = (\pi D/T)$, then we obtain

$$Sr_p = \frac{\pi}{0.1(x / D) + 5.4}. \qquad (6)$$

In other words, Sr_p is inversely proportional to x. We expect that the coefficients in the above equations are functions of the swirl ratio, Sr.

On the other hand, the decays of the maximum amplitude of non-uniformity, ΔC_{Pref} max, are shown in Fig. (15a). These results can be approximated by a power law,

$$\Delta C_{Pref} \text{ max} = A(x / D)^{-m}, \qquad (7)$$

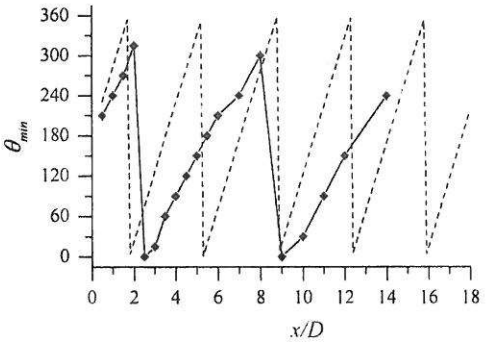

(a) Sr09T

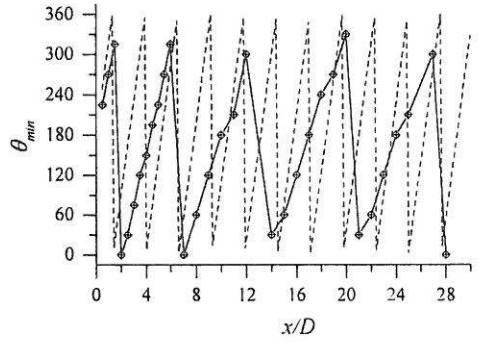

(b) Sr12T

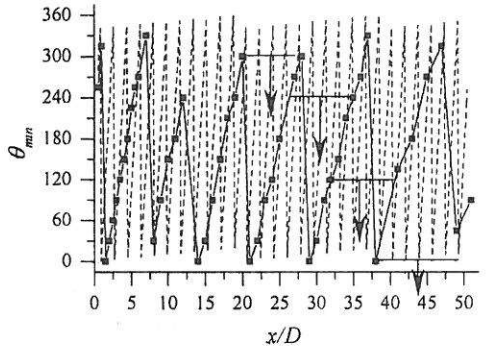

(c) Sr18T

Fig. 13. Periods of the angular motion of the point of minimum wall pressure. Dashed lines show the traces of angular position following the initial swirl helix.

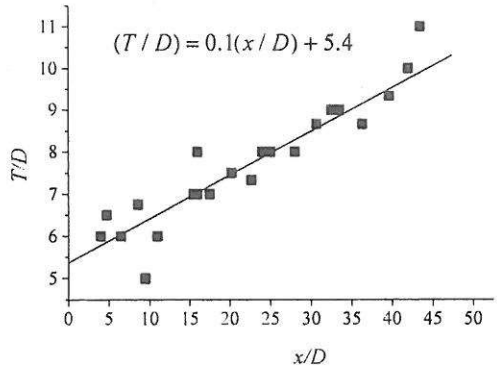

Fig. 14. Stretch of the period of the angular motion of wall pressure non-uniformity in case Sr18T.

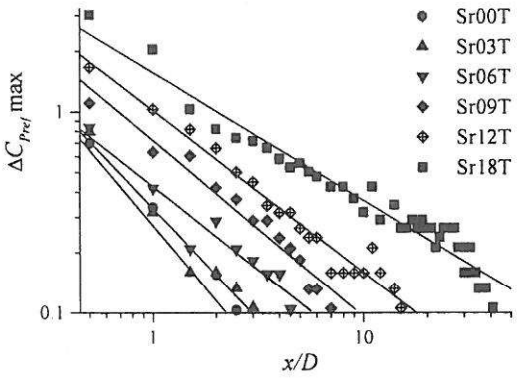

(a)

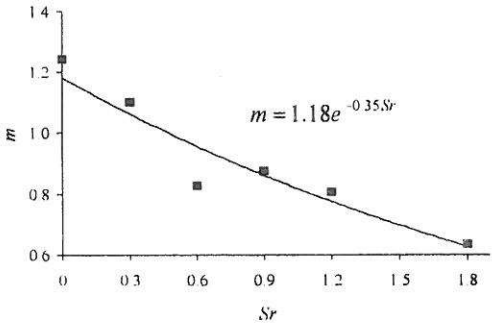

(b)

Fig. 15. Decay of maximum non-uniformity in wall pressure: (a) maximum non-uniformity distribution, (b) decay rate.

where the coefficients for all cases are shown in Table 2. In addition, the decay rate, m, is found to be a function of swirl ratio as shown in Fig. (15b) and can be approximated by the equation $m = 1.18e^{-0.35Sr}$, i.e., an exponential function of swirl ratio.

Case	A	m
Sr00T	0.27	1.24
Sr03T	0.33	1.10
Sr06T	0.43	0.83
Sr09T	0.72	0.88
Sr12T	1.02	0.81
Sr18T	1.57	0.64

Table 2. Decay coefficients for Eq. (7).

Finally, the distributions of the average value of $C_{Pref'}$ over the circumference, $\overline{C_{Pref'}}$, are given in Fig. (16), including cases without tab for comparison. Note, as before, that the reference pressure $P_{ref'}$ is not constant but varies from case to case.

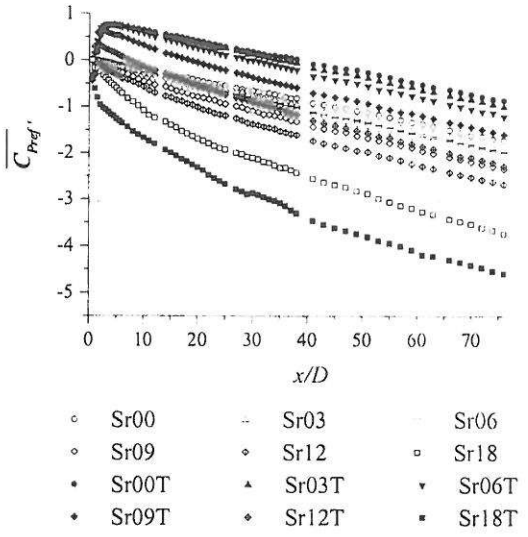

Fig. 16. Distribution of $\overline{C_{Pref'}}$ along pipe axis.

In contrast to cases without tab, cases with tab, except case Sr18T, show recovery in average pressure, i.e., increase in pressure, within the first five diameters. This can be attributed to the blockage effect of the tab. Farther downstream, pressure starts decreasing in a similar fashion to those of cases without tab. However, for case Sr18T, no obvious recovery region is observed. On the other hand, the average pressure starts decreasing at a rate significantly higher than its counterpart, case Sr18. The reason for this characteristics is not yet clear although it suggests a relatively significant suppression of the blockage effect by the swirl. Farther downstream, all the cases without tab exhibit similar drop at a similar rate to their counterparts.

4. Conclusions

Wall pressure distributions in axisymmetric and non-axisymmetric swirling flows are studied. The results for an axisymmetric case show that, unlike a non-swirling flow which has relatively linear average pressure drop from the start, a swirling flow has non-linear drop in the initial region. Specifically, swirl causes fast rate of pressure drop initially, then the rate gradually decreases and approaches linear drop. In addition, the rate of pressure drop also depends on swirl ratio; the higher the swirl, the higher the initial rate, and the minor loss coefficient is found to be proportional to the square of swirl ratio.

On the other hand, when the tab is used to generate segmental wake, or non-uniformity along the circumference, the strength of the wake varies with swirl ratio. Specifically, higher swirl generates stronger wake, the result of which imprints in both pitot and static pressures behind the tab. This effect can be attributed to an increase in effective velocity associated with additional tangential velocity component, which overtakes a decrease in an apparent area of the tab - at least within the range of parameters in the present study.

The segmental blockage of the tab in swirling flows leaves a footprint as non-uniformity in wall pressure along the circumference, which travels in a swirling

motion downstream in the same direction as the swirl. The non-uniformity in wall pressure is traced with the minimum of, and the maximum difference (ΔC_{Pref} max) in, wall pressure. The results show that the recovery length to uniformity in wall pressure (L_u) varies with the square of swirl ratio. The decay of the maximum difference in wall pressure is found to be approximated by a power law, x^{-m}, with the decay rate m by an exponential function of swirl ratio. In addition, in case of maximum swirl (Sr18T), it is found that the decay of swirl ratio for wall pressure (Sr_p) can be approximated by an inverse function of downstream distance. Except for the initial region of pressure recovery, the characteristics of average pressure drop farther downstream in non-axisymmetric swirling cases is similar to those of the axisymmetric counterparts. Nonetheless, in regard to the pressure recovery region, exception is found in the case of highest swirl (Sr18T), where no obvious recovery region is observed.

Finally, it is noted that, besides the applications in various engineering works, the results of this study have direct impact on the design, use, and installation of flow measurement devices.

Acknowledgements

Research grant under The Shell Centennial Education Fund for Graduate Students, Academic Year 1999, from The Shell Company of Thailand Ltd. is gratefully acknowledged.

References

1. Anwer, M., and So, R. M. C., (1989), "Rotation effects on a fully-developed turbulent pipe flow," *Exp. Fluids*, Vol. 8, pp. 33-40.
2. Chue, S. H., (1975), "Pressure probes for fluid measurement," Prog. Aerospace Sci., Vol. 16, No. 2, pp. 147-223.
3. Holzäpfel,F., Lenze, B., and Leuckel, W., (1999), "Quintuple hot-wire measurements of the turbulence structure in confined swirling flows," *J. Fluids Eng.*, Vol. 121, pp. 517-525.
4. Kikuyama, K., Murakami, M., and Nishibori, K., (1983), "Development of three-dimensional turbulent boundary layer in an axially rotating pipe," *J. Fluids Eng.*, Vol. 105, pp. 154-160.
5. Kitoh, O., (1991), "Experimental study of turbulent swirling flow in a straight pipe," *J. Fluid Mech.*, Vol. 225, pp. 445-479.
6. Kline, S. J., (1985), "The purpose of uncertainty analysis," *J. Fluids Eng.*, Vol. 107, pp. 153-160.
7. Kobayashi, T., and Yoda, M., (1987), "Modified k-ε model for turbulent swirling flow in a straight pipe," *JSME Int. J.*, Vol. 30, No. 259, pp. 66-71.
8. Kobkanjanakorn, K., and Bunyajitradulya, A., (1998), "Decays of non-axisymmetric pressure distribution in non-axisymmetric swirling pipe flows: In a straight pipe and downstream of a 90-degree pipe bend," *Proceedings of The Twelfth National Mechanical Engineering Academic Seminar*, Vol. 3, pp. 97-106.
9. Kreith, F., and Sonju, O. K., (1965), "The decay of turbulent swirl in a pipe," *J. Fluid Mech.*, Vol. 22, pp. 257-271.
10. Miau, J. J., Lin, E. C., Chen, Q. S., Chou, J. H., Pan, D., and Lin, C. K., (1996), "Awilring flows in circular-to-rectangular transition ducts," *Exp. Fluids*, Vol. 20, pp. 401-409.
11. Murakami, M., (1961), "Vibration of water-turbine draft tubes," *Trans. ASME Series A*, Vol. 83, p. 36.
12. Murakami, M., and Kikuyama, K., (1980), "Turbulent flow in axially rotating pipes," *J. Fluids Eng.*, Vol. 102, pp. 97-103.
13. Orlandi, P., and Fatica, M., (1997), "Direct simulations of turbulent flow in a pipe rotating about its axis," *J. Fluid Mech.*, Vol. 343, pp. 43-72.
14. Ouazzane A. K., and Barigou M., (1999), "A comparative study of two flow conditioners and their efficacy to reduce asymmetric swirling flow effects on orifice

meter performance," *Chem. Eng. Res. and Des.*, Nov. 1999, pp. 747-753.
15. Parchen, R. R., and Steenbergen, W., (1998), "An experimental and numerical study of turbulent swirling pipe flows," *J. Fluids Eng.*, Vol. 120, pp. 54-61.
16. Rochino, A., and Lavan, Z., (1969), "Analytical investigations of incompressible turbulent swirling flow in stationary ducts," *J. Applied Mech.*, June, 1969, pp. 151-158.
17. Rusak, Z., (1998), "The interaction of near-critical swirling flows in a pipe with inlet azimuthal vorticity perturbations," *Phys. Fluids*, Vol. 10, No. 7, pp. 1672-1684.
18. Rusak, Z., Judd, K. P., and Wang, S., (1997), "The effect of small pipe divergence on near critical swirling flows," *Phys. Fluids*, Vol. 9, No. 8, pp. 2273-2285.
19. Sparrow, E. M., Ramsey, J. W., and Lau, S. C., (1979), "Flow and pressure characteristics downstream of a segmental blockage in a turbulent pipe flow," *J. Fluids Eng.*, Vol. 101, pp. 200-207.
20. Wang, S., and Rusak, Z., (1996), "On the stability of an axisymmetric rotating flow in a pipe," *Phys. Fluids*, Vol. 8, No. 4, pp. 1007-1016.
21. Wang, S., and Rusak, Z., (1997a), "The effect of slight viscosity on a near-critical swirling flow in a pipe," *Phys. Fluids*, Vol. 9, No. 7, pp. 1914-1927.
22. Wang, S., and Rusak, Z., (1997b), "The dynamics of a swirling flow in a pipe and transition to axisymmetric vortex breakdown," *J. Fluid Mech.*, Vol. 340, pp. 177-223.
23. Weske, D. R., and Sturov, G. Y., (1974), "Experimental study of turbulent swirled flows in a cylindrical tube," *Fluid Mech. Sov. Res.*, Vol. 3, pp 77-82.
24. Wu, H. Y., Cheng, H. E., Shual R. J., and Zhou, Q. T., (2000), "An analytical model for decaying swirl flow and heat transfer inside a tube," J. Heat Transfer, Vol. 122, pp. 204-208.
25. Yajnik, K. S., and Subbaiah, M. V., (1973), "Experiments on swirling turbulent flows. Part 1. Similarity in swirling flows," *J. Fluid Mech.*, Vol. 60, pp. 665-687.

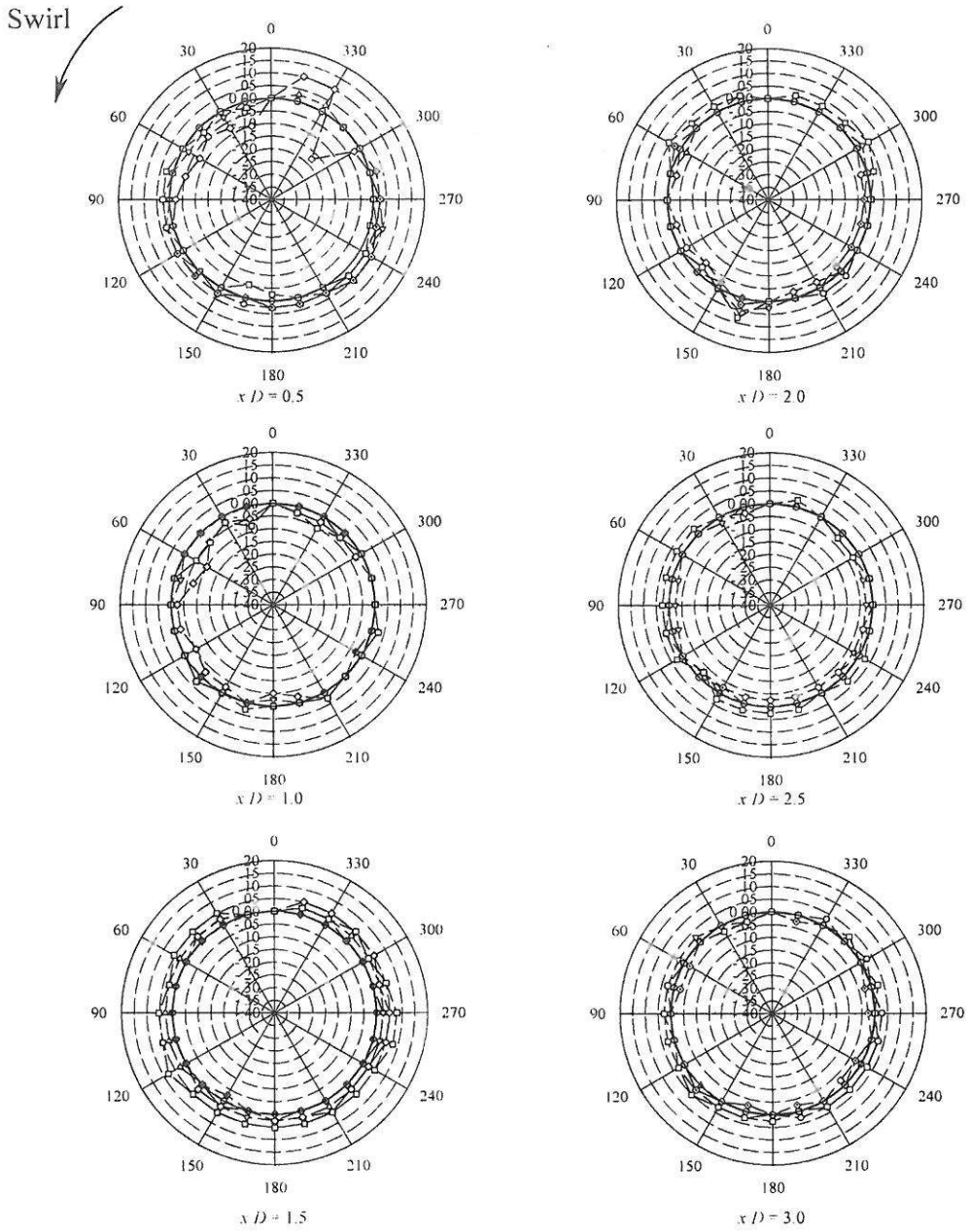

Fig. 8. Wall-pressure distribution (C_{Pref}, looking upstream) for cases without tab, x/D = 0.5-3.0, radial resolution = 0.05. Inner solid circle indicates $C_{Pref} = 0$.

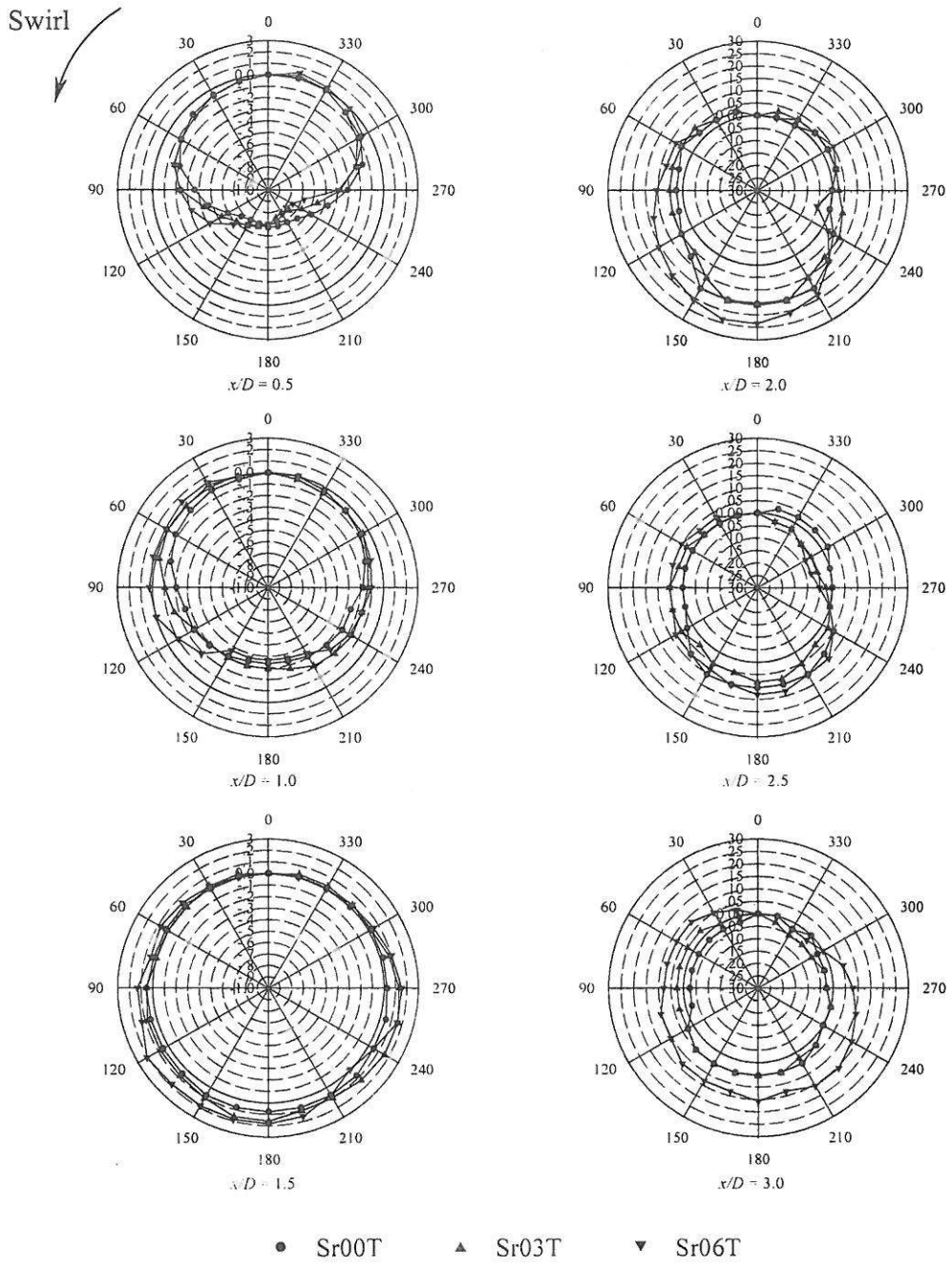

Fig. 11a. Wall-pressure distribution (C_{Pref}, looking upstream) for cases with tab: Sr00T, Sr03T, and Sr06T; x/D = 0.5-3.0. Inner solid circle indicates $C_{Pref} = 0$. Note the change in radial resolution from 0.1 at x/D = 1.5 to 0.05 at x/D = 2.0.

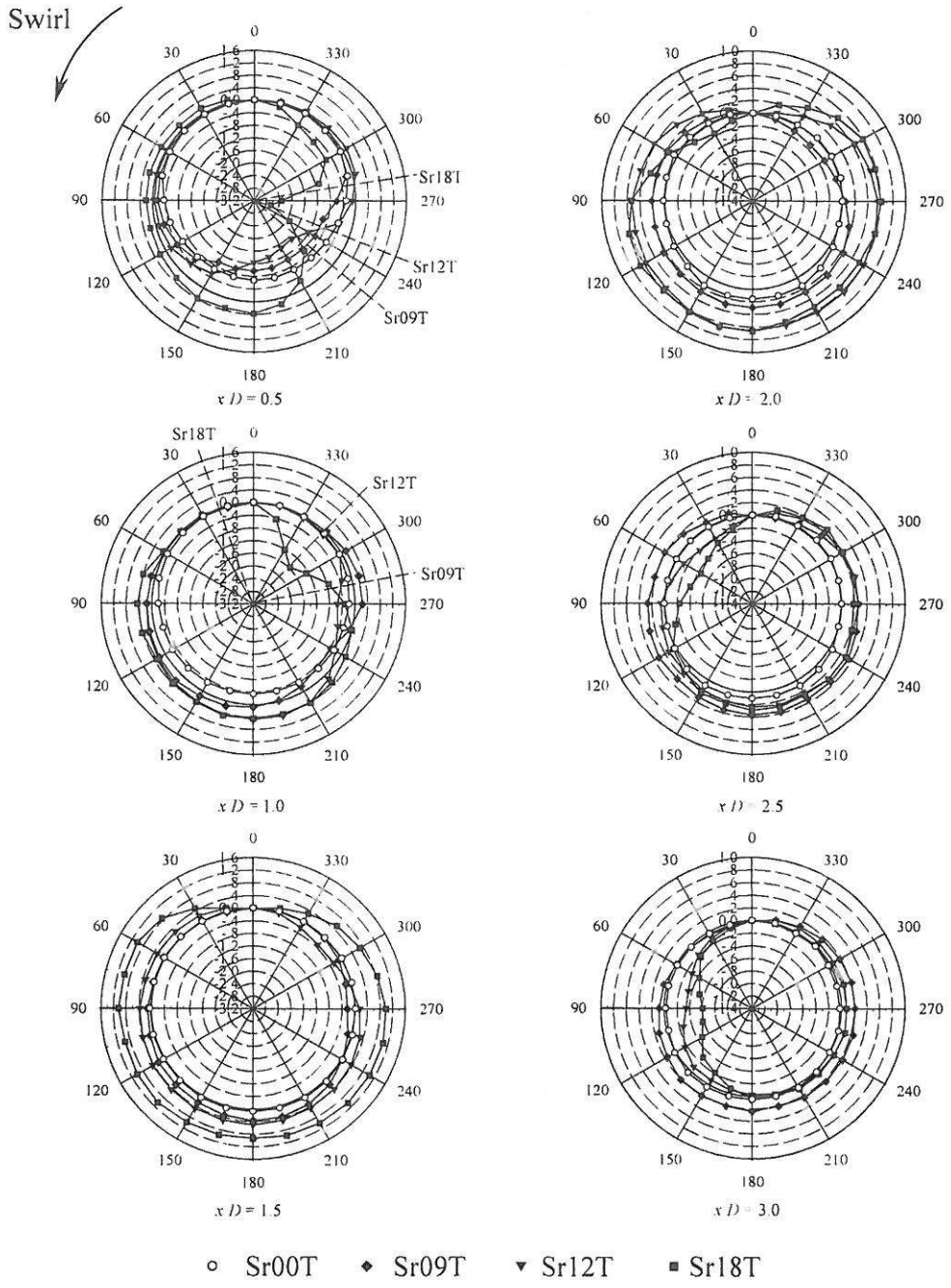

Fig. 11b. Wall-pressure distribution (C_{Pref}, looking upstream) for cases with tab: Sr09T, Sr12T, and Sr18T; case Sr00T is also shown for comparison; x/D = 0.5 - 3.0. Inner solid circle indicates $C_{Pref} = 0$. Note the change in radial resolution from 0.4 at x/D = 1.5 to 0.2 at x/D = 2.0. Dashed lines with case labels indicate the corresponding local angular positions which, starting from tab, follow the initial swirl helix.